JOURNAL OF SPACECRAFT AND ROCKETS
Vol. 46, No. 5, September–October 2009

Review of Options for Autonomous Cislunar Navigation

John A. Christian* and E. Glenn Lightsey†
University of Texas at Austin, Austin, Texas 78758

DOI: 10.2514/1.42819

During the early days of spaceflight, and especially during the Apollo program, significant advances were made in developing methods for navigation in cislunar space. Since then, new technologies and new data processing methods have been created that enable navigation options that were not available during the Apollo era. There are also new requirements associated with NASA's Constellation Program and the Orion spacecraft. Therefore, as NASA prepares to return to the moon, it is instructive to review the options, both new and old, available for cislunar navigation. By comparing the sometimes forgotten techniques used in the early days with the familiar techniques used on modern spacecraft, it is possible to make a more informed selection of the best navigation solutions for future missions to the moon.

Nomenclature

a	=	orbit semimajor axis, km
b	=	measurement bias
c	=	speed of light, km/s
d_a	=	apparent diameter, rad
E	=	eccentric anomaly, rad
e	=	orbit eccentricity
f	=	flux
h_{star}	=	apparent lunar altitude of reference star, km
I	=	ionosphere delay, km
m	=	apparent magnitude
$\mathbf{n}_{\text{star}}$	=	unit vector in direction of reference star (no error sources)
$\hat{\mathbf{n}}_{\text{star}}$	=	unit vector in direction of reference star (with error sources)
PR	=	pseudorange, km
R	=	geometric range, km
R_p	=	radius of planet/moon, km
$\mathbf{r}$	=	position vector of spacecraft, km
$\mathbf{r}_{\text{SF}}$	=	position vector to surface feature, km
T	=	troposphere delay, km
$\mathbf{T}$	=	rotation matrix
t_{SC}	=	time of arrival of pulse from pulsar at spacecraft, s
t_{SSB}	=	time of arrival of pulse from pulsar at solar system barycenter, s
δR_p	=	error in radius of planet, km
ϵ	=	measurement error
η	=	error (vector) in knowledge of the location of a surface feature, km
ν	=	true anomaly, rad
ξ	=	angular measurement between a surface feature and a reference star, rad
ρ	=	range, km
τ	=	error in the measured time of arrival of pulse from pulsar at spacecraft, s
τ_{SSB}	=	error in the predicted time of arrival of pulse from pulsar at spacecraft, s
φ	=	angle between lunar periapsis and projection of antistar direction, rad

Presented as Paper 7265 at the AIAA Guidance, Navigation and Control Conference and Exhibit, Honolulu, HI, 18–21 August 2008; received 17 December 2008; revision received 3 June 2009; accepted for publication 14 June 2009.

*Assistant Instructor, Department of Aerospace Engineering and Engineering Mechanics. Student Member AIAA.

†Professor, Department of Aerospace Engineering and Engineering Mechanics. Associate Fellow AIAA.

I. Introduction

THE increased interest in the moon as a target for robotic and human exploration gives rise to a need for precise orbit determination in cislunar space. The cislunar transfer phase is critical for many mission types and scenarios. For example, precise position knowledge is necessary for a crewed return from the moon due to entry, descent, and landing (EDL) requirements that constrain the spacecraft's position, velocity, and attitude at entry interface [1].

During operations in low Earth orbit (LEO), the data required for navigation may be obtained through traditional spacecraft navigation methods, such as an onboard Global Positioning System (GPS) receiver or radiometric tracking. As the distance between the spacecraft and Earth increases, some of the methods used in LEO become problematic due to design (e.g., GPS signals are designed to transmit toward the Earth) and/or poor geometry. To address this difficulty, past spacecraft operating in cislunar space (e.g., Ranger [2], Lunar Prospector [3], and Apollo [4]) have employed a combination of inertial measurements and inertial state updates from ground tracking. Traditionally, three-axis accelerometers and gyros are used to propagate the state (dead reckoning) between inertial state updates provided from an external source. Between these updates, the integrated solution will drift. The difficulty here lies primarily with the accelerometers and the associated estimate of the spacecraft position; the gyros may be inertially updated using onboard star trackers.

Consider the navigation system for NASA's Orion vehicle [5], the spacecraft expected to return humans to the moon, as a motivating example. For this type of mission, the traditional ground tracking approach (radiometric tracking with up-linked state estimates) is no longer adequate due to the desire for the Orion vehicle to be capable of an autonomous lunar return [6]. Because external updates are required to prevent the dead reckoning state estimate from drifting too far from the true state, autonomous cislunar navigation requires the vehicle to be capable of onboard inertial navigation updates.

The objective of the present research is to investigate navigation solutions that would enable a spacecraft to autonomously navigate in cislunar space. Specifically, the focus is on navigation in the cislunar regime, not in LEO or in low lunar orbit (LLO). Throughout the following discussion, the phrase "autonomous navigation" refers to navigation without contact with Earth. In the case of the Orion example, such a system would permit the safe autonomous return of the Orion vehicle from the moon in the event of a communication system failure.

Note that many of the navigation techniques presented here are not new. What is new, however, are some of the considerations related to implementation in the cislunar regime and the presentation of all of

these techniques in a single location. Also, some of the measurement models are derived at higher fidelity than in prior literature. This study focuses on investigating various measurements that may allow for autonomous state updates. The individual treatment of each of these measurement techniques is for the purposes of a fair side-by-side comparison and is not meant to imply that only one will be used. In practice, it is likely that a few of these external measurements will be combined in a data fusion process. Rather than focus on filter design, measurement combinations, measurement data rates, and other data fusion considerations, the present study focuses on what measurements are available for inclusion in this process.

II. Background and Motivation

A. Overview of Lunar Return Trajectory

Because the focus is placed on cislunar navigation, it is appropriate to consider a reference cislunar trajectory. As a working example for the following studies, consider a spacecraft on a lunar return trajectory (see Fig. 1). This trajectory is representative of the type of return the Orion vehicle is expected to perform. The return trajectory begins with a sequence of three trans-Earth injection (TEI) maneuvers that occur over an approximately 1 day period (see Fig. 1a). Each of the segments in Fig. 1 is separated by one of these TEI maneuvers. These three maneuvers are followed by a long coast period (segment 4), interrupted by trajectory correction maneuvers (TCMs) as necessary. The trajectory shown in Fig. 1, however, does not include any TCMs. The coast period shown in segment 4 has a duration of approximately 3.5 days.

Constellation program requirements dictate that the Orion spacecraft shall be capable of autonomously returning to Earth at any time during the mission. As a direct result, the navigation system must be capable of autonomously supporting a return to Earth throughout all mission phases. Specifically, the vehicle must be capable of safely returning the crew to Earth in the event that ground updates of the inertial state are no longer available. The driving requirement during an emergency return is expected to be the entry flight path angle (FPA). Recall that the FPA is defined as the angle between the velocity vector and the local horizontal [7]. Although the required navigation solution for the entry FPA is expected to be approximately 0.1 deg (3σ), the acceptable entry FPA error may be significantly larger for autonomous (off-nominal) returns.

B. Inertial Navigation

Inertial navigation represents one extreme in the spectrum of autonomous navigation. Inertial navigation allows the spacecraft to track its position and velocity as a function of time without requiring measurements from the outside environment. Because accelerometers do not measure the acceleration due to gravity, propagation of the spacecraft position and velocity is dependent on a gravity model stored in the spacecraft computer. When nongravitational forces are applied to the vehicle (e.g., propulsive maneuver, waste venting, etc.), the total acceleration may be computed by combining the predicted gravitational acceleration from the gravity model with the sensed accelerations measured by the accelerometers. The spacecraft state vector may be tracked over time by integration of these accelerations from some set of initial conditions.

Unfortunately, knowledge of the gravity field is imperfect and the gravity models used for real-time applications require approximations that may introduce significant errors for long propagation periods (e.g., truncation of the spherical harmonic representation of the Earth and moon gravity fields). Further, there are numerous sources of error in the acceleration measured by the accelerometer. An error model for a typical accelerometer is given by [8]

$$\tilde{\mathbf{a}} = [\mathbf{I}_{3\times 3} + \mathbf{S}_a + \Gamma_a](\mathbf{a} + \boldsymbol{\beta}_a + \mathbf{w}_a) \tag{1}$$

where $\mathbf{S}_a$ is the scale-factor error matrix, Γ_a is the misalignment error matrix, $\tilde{\mathbf{a}}$ is the measured acceleration, $\mathbf{a}$ is the true acceleration, $\boldsymbol{\beta}_a$ is the accelerometer bias, and $\mathbf{w}_a$ is zero mean white noise.

Because of these errors, the solution achieved by simply integrating the measured/predicted accelerations accumulates error over time and the system requires external updates to maintain an accurate estimate of the state. During the Apollo program, these external updates were primarily provided by ground-based tracking. The capability for autonomous navigation was retained as a backup, but not regularly used because of extremely high demands on crew time.

C. Sources of Autonomous Inertial Navigation Updates

Determining the degree of autonomy that should be incorporated into a spacecraft is an important design decision. The desire for autonomous lunar navigation is a long standing issue (especially in human spaceflight) that has led to numerous studies since the 1960s [9–11]. Autonomous navigation techniques (mostly optical) have also been tested and widely used during the planetary approach phase of robotic exploration missions [12–15]. Because the required degree of autonomy will vary from mission to mission, a spectrum of navigation solutions is considered (see Fig. 2).

The approaches presented toward the right half of Fig. 2 represent solutions that would allow for autonomous inertial navigation updates. These solutions rely primarily on optical measurements. In such a scenario, the spacecraft would detect natural objects, passive surface beacons, or artificial satellites for which precise position data are available. Then, by coupling accurate angular measurements with precise target position information, the resulting data may be used to produce an estimate of the spacecraft's inertial position [16]. Further, the use of natural targets would allow for inertial state updates without requiring the emplacement of additional space-based assets and without the need for contact or communication with the Earth.

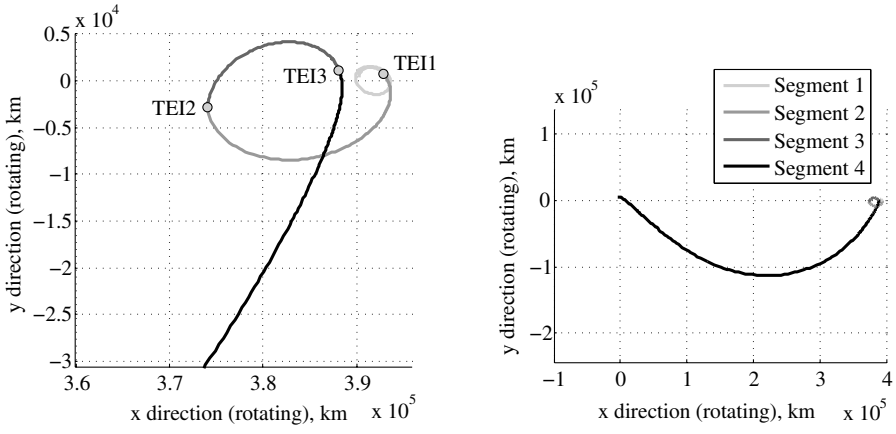

a) Zoom in near the moon **b) Overview of entire trajectory**

Fig. 1 Representative lunar return trajectory as seen in a rotating frame with the *x* axis along the Earth–moon line and the origin at the center of the Earth. Data supplied by NASA Johnson Space Center.

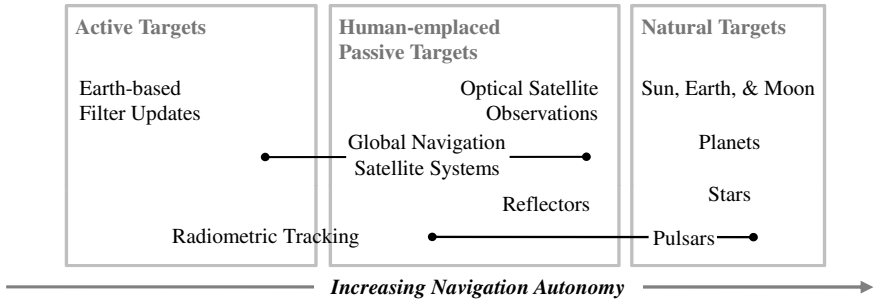

Fig. 2 Potential navigation solutions for inertial updates during lunar return.

Use of natural targets also helps to create a robust navigation architecture. The observation of man-made targets may introduce additional maintenance, infrastructure, overhead, and failure modes not seen with natural targets. It should also be noted that, despite these advantages, natural targets rarely have the precision associated with man-made systems specifically designed for navigation.

III. Analysis of Promising Sources for Inertial Navigation Updates

The cislunar navigation methods described next appear to be the most promising for near-term implementation. It is unlikely that these measurements will be used in isolation. Instead, it is likely that the information from more than one of these techniques will be combined in a data fusion process.

A. Centroid and Apparent Diameter of Earth and Moon

The most prominent natural targets in cislunar space are the sun, Earth, and moon. Because of proximity, size, and geometry, the Earth and the moon are expected to be among the best sources of data for navigation. Perhaps the coarsest angular measurement that may be taken with these bodies is an estimate of location of the body centroid or the center of brightness (similar in concept to the approached used by the Deep Impact mission) [14]. Simply determining the direction to the centroid of the sun, Earth, and moon could be enough to generate a position fix in cislunar space. Such a measurement may be difficult to make, however, due to adverse lighting conditions or phases of both the Earth and moon.

Other coarse measurements include observations of the Earth or moon horizon [17]. Given the large distances between the spacecraft and the Earth (or moon), detection of the horizon will likely be done through image analysis rather than with traditional horizon sensors. Analysis of an image that contains the Earth or moon may be used to estimate the direction to that body as well as its apparent diameter. Given knowledge about the size and shape of the Earth and moon, apparent diameter measurements could be used to estimate the range.

Because the moon has no atmosphere, the sunlit surface has a crisp horizon, making it relatively easy to accurately detect and measure surface features or the horizon location. The Earth, on the other hand, has an atmosphere that obscures the horizon to an extent that it may not be seen from orbit. Instead, there is only a fuzzy band with no clear visual feature to support easy measurement. Despite this difficulty, Apollo astronauts demonstrated their ability to measure a point somewhere in the blurry horizon with repeatability on the order of only a few kilometers [18]. It is possible, although not trivial, that a system could be designed to reproduce the astronauts' performance autonomously. Alternatively, instead of using the visible spectrum to locate the Earth's horizon, the CO_2 layer of the atmosphere may be observed in the infrared spectrum (14.0–16.3 μm wavelength). The CO_2 layer will form a crisper horizon than achievable in the visible band and is the method of choice for locating the horizon with traditional LEO horizon sensors. A sensor capable of performing this task would be similar to existing infrared static earth sensors that are presently able to achieve apparent diameter estimates with a total rms error on the order of 0.03 deg (108 arcseconds) in LEO [19].

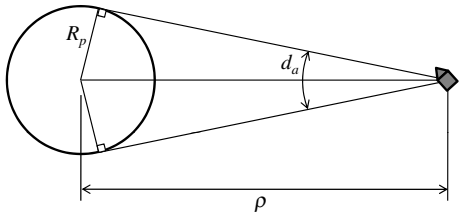

Fig. 3 Geometry for apparent diameter measurement.

There are numerous measurement models, of varying sophistication, that one may use to estimate the performance of this technique. A simple model is presented here to gain an appreciation for the sensitivity of this approach to measurement errors. Begin by assuming that an image processing algorithm produces the apparent diameter of the Earth or moon as an angular measurement. Then, from geometry (see Fig. 3), a relationship between the angular apparent diameter measurement d_a and the range to the body of interest ρ is given by

$$d_a = 2\sin^{-1}\left(\frac{R_p}{\rho}\right) \tag{2}$$

where R_p is the radius of the planet. When error effects are included, Eq. (2) may be rewritten as

$$d_a = 2\sin^{-1}\left(\frac{\hat{R}_p}{\rho}\right) + b + \epsilon \tag{3}$$

where $\hat{R}_p$ is an estimate of the planet radius given by $\hat{R}_p = R_p + \delta R_p$, δR_p is the error in the radius of the planet, b is the measurement bias, and ϵ is the measurement error.

Taking the Taylor series expansion of the measurement model around a reference solution allows the expression in Eq. (3) to be linearized. Taking the partial derivative of the scalar measurement with respect to the $n \times 1$ column vector state yields the $1 \times n$ measurement sensitivity matrix $\mathbf{H}$. Errors are frequently assumed to behave in a linear fashion around the reference solution such that the measurement sensitivity matrix may be used to map errors in the state estimate to errors in the measurement. This approach is common in many types of filters (e.g., Kalman filter) and is discussed extensively in the literature [20–22]. Therefore, for a generic state vector $\mathbf{x}$, consider a measurement $\mathbf{y}$ that is a nonlinear function of the state, $\mathbf{y} = h(\mathbf{x})$. Under these conditions,

$$\delta\mathbf{y} \approx \frac{\partial h(\mathbf{x})}{\partial \mathbf{x}}\delta\mathbf{x} = \mathbf{H}\delta\mathbf{x} \tag{4}$$

where $\delta\mathbf{x}$ is the deviation of the state from the reference and $\delta\mathbf{y}$ is the deviation of the measurement from the reference. For the case of an apparent diameter measurement, the relevant partial is given by

$$\frac{\partial d_a}{\partial \mathbf{r}} = -\left(\frac{2\hat{R}_p}{\mathbf{r}^T\mathbf{r}\sqrt{\mathbf{r}^T\mathbf{r} - \hat{R}_p^2}}\right)\mathbf{r}^T \tag{5}$$

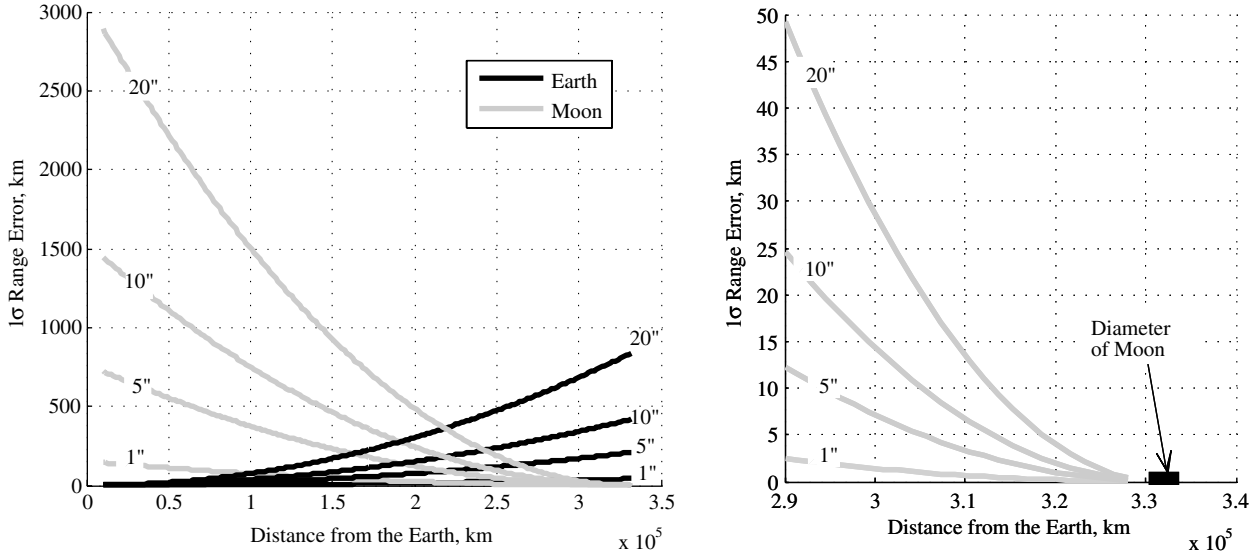

a) Overview of errors for earth/moon apparent diameter measurements b) Zoom in near the moon

Fig. 4 Simple simulation of accuracy of optical ranging measurements to the Earth and moon for 1σ apparent diameter measurement errors of 1–20 arcseconds.

where **r** is the spacecraft position vector with respect to the observed body (note that $\rho = \|\mathbf{r}\|$). This partial allows an error in the spacecraft position to be mapped into an error in the angular apparent diameter.

A simulation was performed to gain a better feel for the performance of a system using the measurement model given in Eq. (2). In this simulation (see Fig. 4 for results), the 1σ error in estimated range to the Earth and to the moon is computed as a function of distance from the Earth and apparent diameter measurement error. The 1σ apparent diameter measurement errors were varied from 1 to 20 arcseconds. The errors associated with this method are too large in the intermediate space between the Earth and the moon for most applications, even in the best measurement case. However, as the spacecraft becomes closer to the Earth or moon, the range errors become smaller and this approach becomes a viable method for obtaining coarse range estimates with 1σ errors on the order of a few kilometers.

The error in the apparent diameter measurement is highly variable and is a function of the specifications of the instrument being used, the range to the moon, and other environmental parameters. To help understand what is feasible with such an approach, consider a system that works as follows. Using an image of the moon taken by a camera with a limited field of view, an algorithm creates a set of points that best estimate the location of the lunar horizon. Next, an arc is placed through this set of points, as shown in Fig. 5a. In this analysis, a circular arc is assumed. Note that it is straightforward to extend this algorithm to use elliptical arcs instead. Using this approach, an analysis was performed to look at the sensitivity of the quality of the estimate to the number of points used and the size of the lunar horizon arc that was captured in the image. If it is assumed that the location of the horizon may be identified within 10 km (1σ), then the results are as shown in Fig. 5b. The largest errors introduced by fitting a circular arc through the data points are expected to come from measurement error, unmodeled local topography, and the fact that the moon is not a perfect sphere. Note that this methodology does not require the entire moon (or Earth) to be in the imager's field of view. Although phases of the moon may limit the size of the horizon arc that may easily be detected, it is not expected to be a significant contributor to error. The algorithm needs only to fit a curve to the lighted portion of the horizon to estimate the apparent diameter and centroid.

B. Angular Measurements Between Surface Features and Reference Stars

More sophisticated approaches may take advantage of known surface features on the Earth or the moon. Previous work has demonstrated that angular measurements between known stars and known landmarks (or the horizon) on the Earth or moon may be used for cislunar navigation [9]. It is important to note, however, that implementation of such a system may require significant crew involvement and/or complicated image recognition software. Despite this drawback, this approach was demonstrated during Apollo [18]. Two images from Apollo Guidance, Navigation, and Control (GNC) training documentation, shown in Fig. 6, pictorially describe the approach used by Apollo astronauts [23].

The Apollo GNC system was originally designed to be capable of supporting a return to Earth completely independent of Earth-based resources. Unfortunately, limitations in onboard computer memory forced some functions to be shifted to ground tracking facilities and mission control [18]. Even after this reduction in capability, the crew maintained sufficient onboard navigational capability to return to Earth in the event of a communications system failure. The key instrument that enabled this onboard capability was a specially designed sextant used to measure the angle between a selected Earth or moon feature and a reference star. This device, operated manually by one of the astronauts, was capable of making angular measurements with accuracy on the order of 10 arcseconds (made possible through a 28 power eyepiece) [18]. Unfortunately, the field of view for the high-power eyepiece was so small that a wide field scanning telescope was also required. Schematics of the sextant and scanning telescope obtained from the NASA History Division[‡] (Fig. 7) illustrate how the angle between the Earth/moon landmark and the reference star was actually measured. Astronauts claim to have found the star–horizon measurement easier to obtain than the star–landmark measurement. In practice, the trunnion angle was manually adjusted by the astronaut until the image of the reference star was superimposed on the lunar horizon (similar to how a traditional sextant works for Earth applications). When a measurement was ready to be recorded, the astronaut could press a "mark" button to record the time and trunnion angle. This information was passed to the spacecraft computer where Program 23 (P-23), the Cislunar Navigation Program [24,25], would determine the state update. If the state update was within the expected bounds, the measurement was permitted to update the state.

The performance of this system was demonstrated on Apollo 8 when Jim Lovell took over 200 sextant sightings and was able to calculate closest approach to the moon (using only onboard resources) within 2.5 km of that computed by postflight analysis [18].

[‡]Woods, D., and Brandt, T., "Apollo Flight Journal, Apollo 16, Day One Part Two: First Earth Orbit," NASA History Div., http://history.nasa.gov/ap16fj/02_Day1_Pt2.htm [cited 24 January 2008].

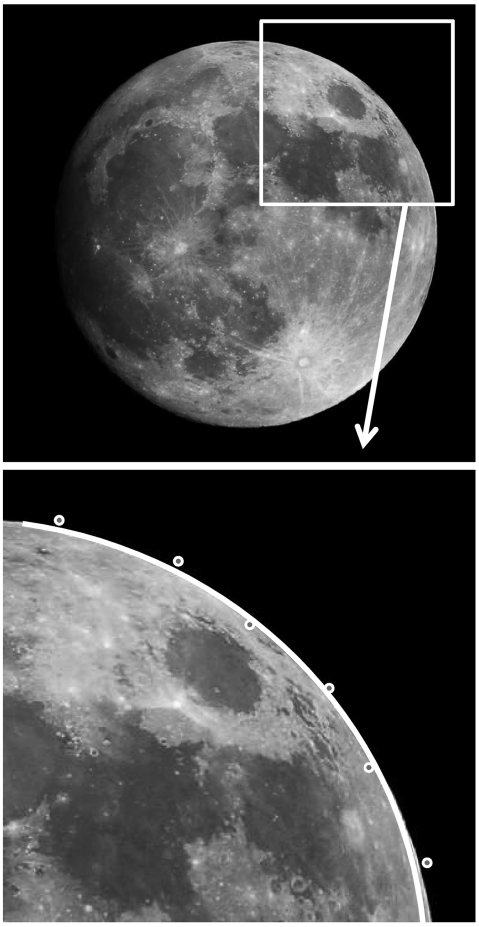

a) The location of the lunar horizon is estimated from an image of the moon

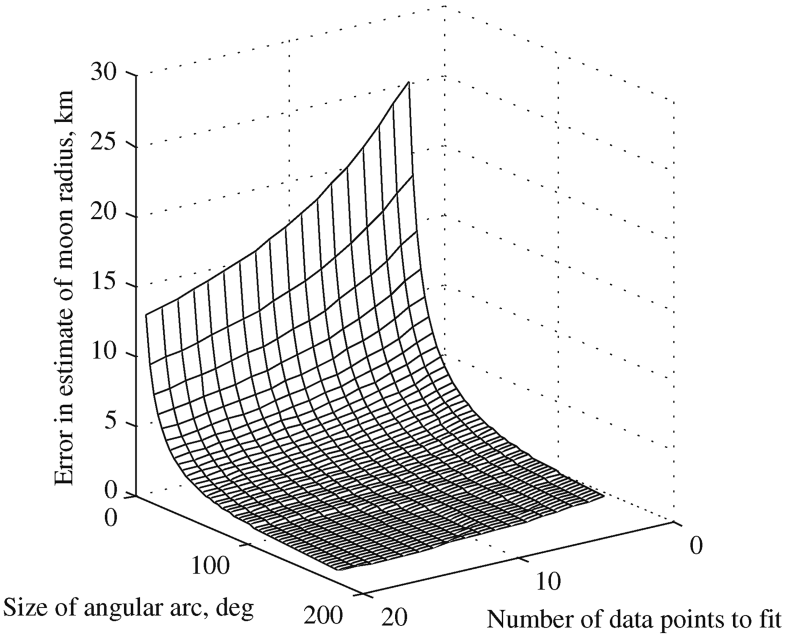

b) Error in the estimate of the moon's radius

Fig. 5 Apparent diameter estimation.

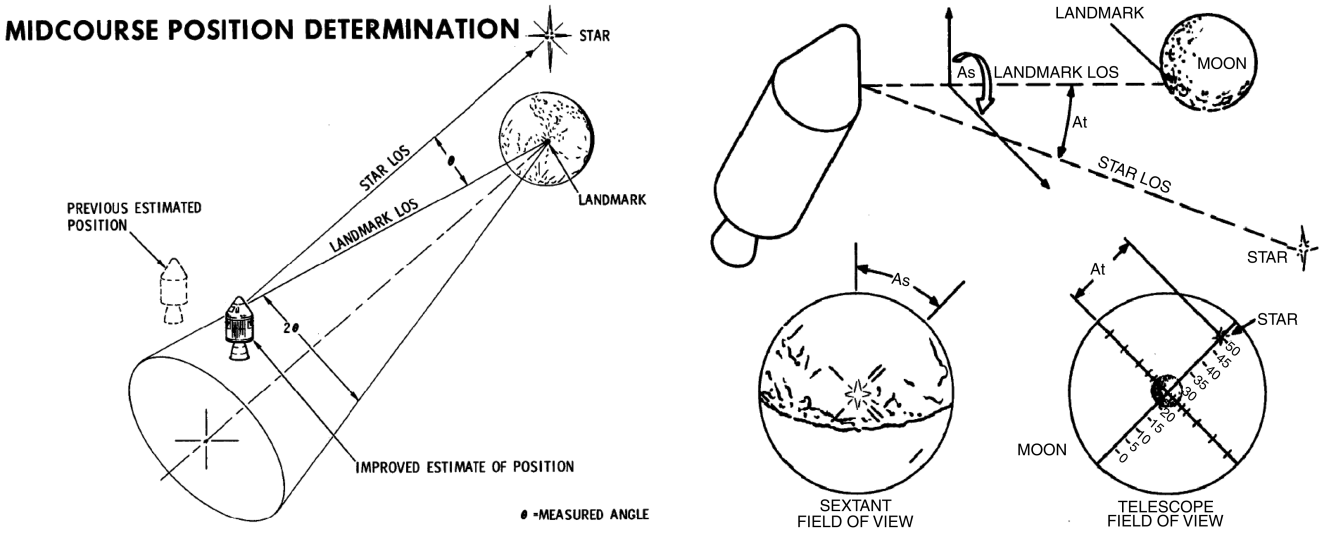

Fig. 6 Images from Apollo training documentation explaining how to use angular measurements between lunar surface features and a reference star for cislunar navigation [23].

During the return, Lovell also demonstrated that this method provided sufficient accuracy to meet the reentry requirements [18,26]. This capability was demonstrated again during later Apollo missions. Data from Apollo 15 (see Table 1) [24,27] demonstrate that the onboard FPA estimates were sufficient to meet the reentry requirements (error of ± 0.5 deg desired, ± 1 deg required). Note that the difference between the ground-based entry FPA estimates and onboard entry FPA estimates collapse to below the reentry requirement as time approaches entry interface (entry interface occurs 308.5 h after liftoff).

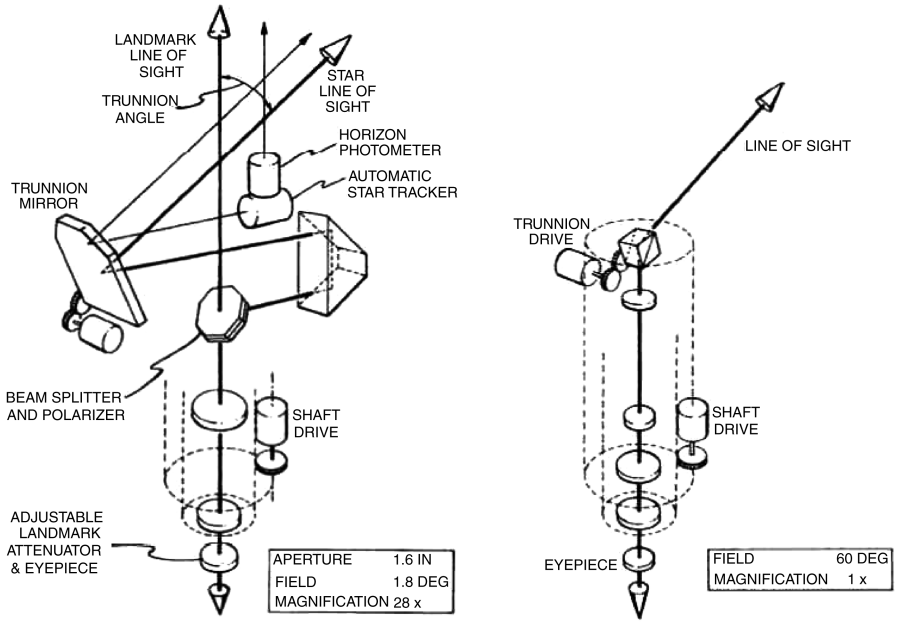

Fig. 7 Schematic of the sextant (left) and scanning telescope (right) used for autonomous navigation in the Apollo command module.[‡]

Although not in the Earth/moon system, there are many similar examples from the history of robotic exploration. The Mariner 9 spacecraft, for example, successfully performed a navigation experiment using optical images of Phobos, Demos, and background stars during its Mars approach [12]. Or, more recently, the MESSENGER spacecraft used images of Mercury and the background starfield for navigation during three Mercury flybys and the final Mercury orbit insertion [28].

From the strategy just described, and as shown graphically in Fig. 8, a basic measurement model may be developed. From the figure, it is straightforward to show that the angular measurement between the surface feature and reference star is given by

$$\xi = \cos^{-1}\left[\left(\frac{\mathbf{r}_{\mathrm{SF}} - \mathbf{r}}{\|\mathbf{r}_{\mathrm{SF}} - \mathbf{r}\|}\right) \cdot \mathbf{n}_{\mathrm{star}}\right] \tag{6}$$

where $\mathbf{r}_{\mathrm{SF}}$ is the position vector from the center of the planet to the surface feature, $\mathbf{r}$ is the position vector from the center of the planet to the spacecraft, and $\mathbf{n}_{\mathrm{star}}$ is the unit vector in the direction of the line of sight of the reference star. When error effects are included, Eq. (6) may be expanded and rewritten as

$$\xi = \cos^{-1}\left[\left(\frac{\hat{\mathbf{r}}_{\mathrm{SF}} - \mathbf{r}}{\|\hat{\mathbf{r}}_{\mathrm{SF}} - \mathbf{r}\|}\right) \cdot \hat{\mathbf{n}}_{\mathrm{star}}\right] + b + \epsilon \tag{7}$$

where $\hat{\mathbf{r}}_{\mathrm{SF}}$ is an estimate of the location of the surface feature given by $\hat{\mathbf{r}}_{\mathrm{SF}} = \mathbf{r}_{\mathrm{SF}} + \eta$, η is the error (vector) in the knowledge of the location of the surface feature, b is the measurement bias, ϵ is the measurement error, and $\hat{\mathbf{n}}_{\mathrm{star}}$ is the unit vector in the direction of the line of sight of the reference star including sources of measurement error:

$$\hat{\mathbf{n}}_{\mathrm{star}} = \mathbf{T}(\boldsymbol{\zeta})\mathbf{T}(\boldsymbol{\sigma})\mathbf{n}_{\mathrm{star}} \tag{8}$$

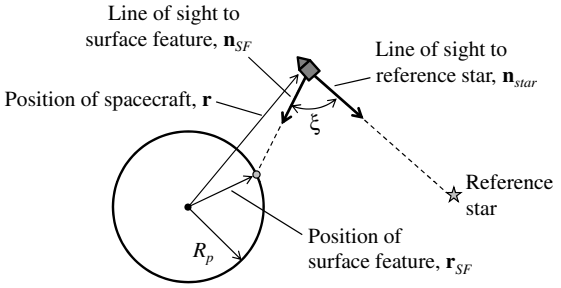

Fig. 8 Geometry for angular measurement between surface feature and reference star.

where $\mathbf{T}(\boldsymbol{\zeta})$ is a rotation matrix that describes the alignment error of the sensor and $\mathbf{T}(\boldsymbol{\sigma})$ is a rotation matrix that describes the error in the catalog position of the reference star.

If this approach is to be automated, the system must have the capability to identify and track stars and surface features without crew involvement. Automation is clearly necessary if such a system is to be used on a robotic spacecraft. On a crewed spacecraft, automating this process should reduce crew workload, reduce sources of human error, and remove the difficulty the Apollo astronauts experienced with using the space sextant to measure the angle between a surface feature and a reference star. The ability to identify and track stars is a well-understood problem and is routinely preformed in star trackers [29]. Lunar surface feature tracking is a significantly more complicated task. A large body of work exists in the literature regarding navigation in LLO and in lunar descent/landing using optical information and terrain relative navigation [30–34]. It remains to be determined how effective these techniques would be at identifying the line-of-sight unit vector to a known

Table 1 Comparison between Apollo 15 onboard (autonomous) and ground-based estimate of entry flight path angle [24]

Time to entry interface	Onboard entry FPA	Ground-based entry FPA	Entry FPA difference	$\pm 1\sigma$ ground-based entry FPA
−58.2 h	−7.23 deg	−6.69 deg	−0.54 deg	1.74 deg
−43.7 h	−7.22 deg	−6.69 deg	−0.53 deg	0.50 deg
−31.5 h	−6.56 deg	−6.50 deg	−0.06 deg	0.30 deg
−22.0 h	−6.55 deg	−6.50 deg	−0.05 deg	0.30 deg
−19.0 h	−6.61 deg	−6.50 deg	−0.11 deg	0.30 deg
−6.0 h	−6.26 deg	−5.82 deg	−0.44 deg	0.13 deg
−1.4 h	−6.80 deg	−6.49 deg	−0.31 deg	0.10 deg

surface feature in cislunar space (i.e., large distances from the moon) for use in generating a measurement of the angle ξ in Fig. 8. It is possible that reflectors or markers may be placed on the lunar surface to aid in the identification of specific points.

As before, the measurement sensitivity matrix [described in Eq. (4)] may be computed for this measurement. Taking the partial of the measurement ξ with respect to the spacecraft position vector $\mathbf{r}$ [recall that, as with Eq. (6), $\mathbf{r}$ is measured with respect to the observed celestial body] yields

$$\frac{\partial \xi}{\partial \mathbf{r}} = \{(\hat{\mathbf{r}}_{SF}-\mathbf{r})^T(\hat{\mathbf{r}}_{SF}-\mathbf{r}) - [(\hat{\mathbf{r}}_{SF}-\mathbf{r})^T\hat{\mathbf{n}}_{star}]^2\}^{-\frac{1}{2}} \cdot \left[\hat{\mathbf{n}}_{star}^T - \frac{(\hat{\mathbf{r}}_{SF}-\mathbf{r})^T\hat{\mathbf{n}}_{star}}{(\hat{\mathbf{r}}_{SF}-\mathbf{r})^T(\hat{\mathbf{r}}_{SF}-\mathbf{r})}(\hat{\mathbf{r}}_{SF}-\mathbf{r})^T\right] \tag{9}$$

In addition to the direct estimation of position, multiple images separated in time of the moon (or Earth) and background starfield may be compared to create a velocity estimate. It has also been suggested that the motion of an unknown surface feature may be used for navigation purposes [35,36]. The use of unknown surface features as navigation aids is a potentially promising approach for navigation in LLO. Unfortunately, however, this technique has only been explored for low altitude satellites orbiting a planet; at the present time, it is not known if changes in geometry over the course of the lunar return would be sufficient to provide meaningful navigation information. This suggests that the use of unknown surface feature tracking is more promising for LLO operations than for cislunar navigation.

C. Star Occultation by Earth or Moon

Another technique involves the occultation of stars by the Earth or moon [37–39]. Here, rather than measuring the angle between surface features and stars, the time at which stars are eclipsed by the Earth or moon is measured. Unfortunately, time is also the independent variable in the dynamic model, which makes directly implementing this measurement into a filter problematic. A number of approaches have been proposed to deal with this problem. Psiaki and Hinks [39] propose a transformation where the apparent altitude of the reference star above the lunar surface is measured instead of time (see Fig. 9). Occultation occurs when the apparent lunar altitude of the reference star h_{star} is zero. As before, a measurement model may be developed through geometry:

$$h_{star} = \|\mathbf{r} - (\mathbf{r}\cdot\mathbf{n}_{star})\mathbf{n}_{star}\| - R_p \tag{10}$$

where $\mathbf{r}$ is the position vector from the center of the planet to the spacecraft, $\mathbf{n}_{star}$ is the unit vector in the direction of the line of sight of the reference star, and R_p is the radius of the planet. Adding error effects yields

$$h_{star} = \|\mathbf{r} - (\mathbf{r}\cdot\hat{\mathbf{n}}_{star})\hat{\mathbf{n}}_{star}\| - \hat{R}_p + b + \epsilon \tag{11}$$

where $\hat{R}_p$ is an estimate of the planet radius given by $\hat{R}_p = R_p + \delta R_p$, δR_p is the error in the radius of the planet, b is the measurement bias, ϵ is the measurement error, and $\hat{\mathbf{n}}_{star}$ is as given by Eq. (8).

Psiaki and Hinks suggest that this approach is capable of producing estimates of the spacecraft's absolute position with an error on the order of 70 m per axis and absolute velocity errors on the order of 0.045 m/s per axis [39]. These results assume the following: a nearly circular lunar orbit (altitude of 315 km), the lunar topography is known to within 100 m, the gravity model is known to within 10^{-5} m/s^2, and the star tracker timing has a 1σ error of 1 ms and contains a catalog of the 2000 brightest stars. Here, it is important to note that the assumed gravity model (acceleration errors less than 10^{-5} m/s^2 in LLO) is better than any currently existing lunar gravity model. To obtain the results described earlier, a mission such as the currently planned Gravity Recovery and Interior Laboratory mission would be required to obtain a better lunar gravity model. Further, the magnitude of these errors is expected to increase as the spacecraft moves farther away from the moon.

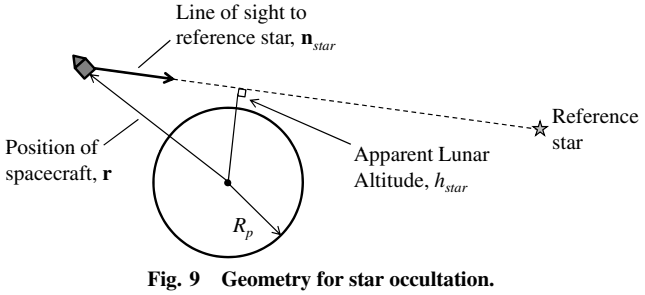

Fig. 9 Geometry for star occultation.

In another approach developed by Landgraf et al. [38], it is assumed that the spacecraft is on a hyperbolic lunar approach trajectory. In their 2006 paper, the authors suggest using two-body orbital mechanics and geometry to determine the true anomaly at which an occultation should occur. Although the following measurement model and derivation differs significantly from that of Landgraf et al., it was inspired by their approach.

Consider a star that will be eclipsed by a planet. If the star is sufficiently far away from the planet, the region where the star is eclipsed by the planet forms a cylinder extending away from the reference star (Fig. 10). Now suppose the spacecraft of interest is approaching the planet on a hyperbolic orbit. The intersection of this orbit plane and the 3-D cylindrical eclipse region will form a 2-D elliptical eclipse region in the orbit plane (Fig. 11). The intersection of the hyperbolic orbit with the elliptical eclipse region marks the true anomaly where a star occultation begins and ends.

From geometry, it can be shown that the semimajor axis of the eclipse region $a_{eclipse}$ is given by $a_{eclipse} = R_p/\sin\theta$, where θ is the angle between the vector pointing to the reference star and the spacecraft orbital plane. The semiminor axis $b_{eclipse}$ is given by $b_{eclipse} = R_p$. A little further geometry demonstrates that

$$x_{eclipse} = a_{eclipse}\cos(E_{eclipse}) = r_{eclipse}\cos(\nu+\varphi) \tag{12}$$

$$y_{eclipse} = a_{eclipse}\sin(E_{eclipse}) = r_{eclipse}\sin(\nu+\varphi) \tag{13}$$

where $E_{eclipse}$ is the eccentric anomaly of the eclipse ellipse, ν is the true anomaly, and φ is the angle between the lunar periapsis and the projection of the antistar direction on the orbital plane. Note that all angles in Eqs. (12) and (13) are taken from the center of the planet, which is located at the geometric center of the eclipse ellipse. Additional manipulation demonstrates that

$$r_{eclipse}^2 = \frac{R_p^2}{\sin^2\theta + \cos^2\theta\sin^2(\nu+\varphi)} \tag{14}$$

where R_p is the radius of the planet (in this case, the moon). By setting the radius equal to the well-known polar equation for a two-body orbit, $r = p/[1+e\cos(\nu)]$, the location at which a specified reference star is eclipsed by the moon is given by the solution to

$$R_p^2[1+e\cos(\nu)]^2 = p^2[\sin^2\theta + \cos^2\theta\sin^2(\nu+\varphi)] \tag{15}$$

where p is the orbit semilatus-rectum. Depending on the geometry, zero, one, or two real solutions to ν exist. Of particular interest is the case of Eq. (15) in which two real solutions to ν exist: one corresponding to the true anomaly where the reference star enters the eclipse of the moon and the other corresponding to the true anomaly where the star leaves the eclipse of the moon. Although they use a different measurement model than that shown in Eq. (15), Landgraf et al. suggest that this approach may yield position fixes on the order of 1 km [38]. Further, their work demonstrates that the sensor must be capable of observing stars of magnitude 7 to provide enough stars for navigation. Although such a system is conceptually possible, there may be difficulties in determining the exact time a star of magnitude 7 moves behind the extremely bright (magnitude −12.6) surface of the moon. Some of these issues may be avoided by only looking at occultations on the dark side of the moon.

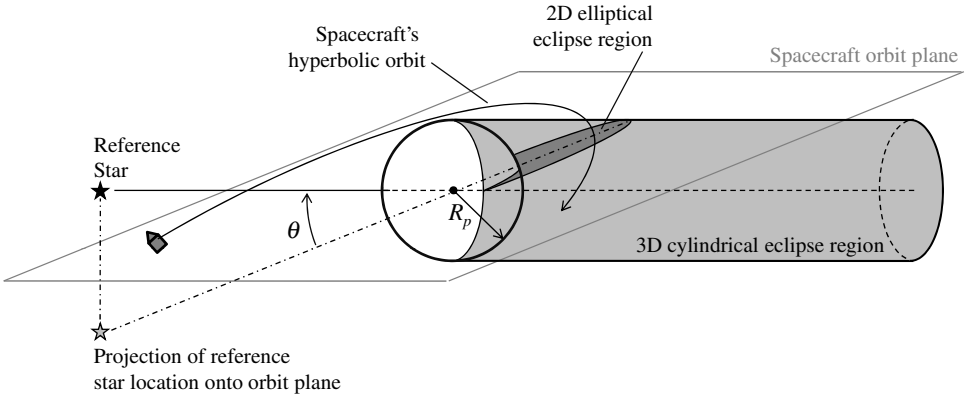

Fig. 10 Three-dimensional geometry for star occultation.

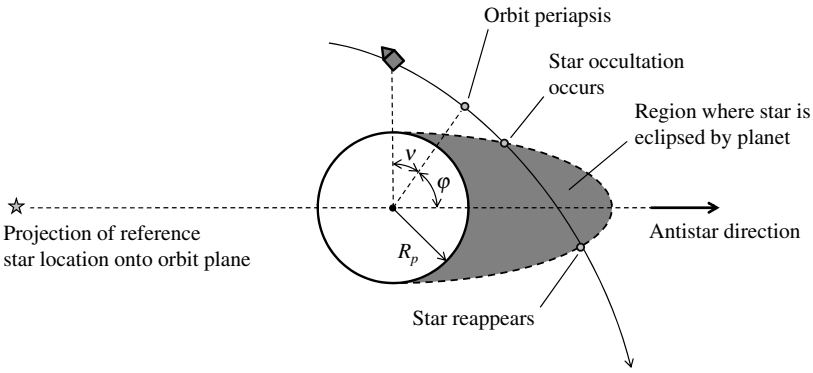

Fig. 11 Geometry for star occultation as seen in the spacecraft orbit plane.

Although the previous discussion focuses on occultations of stars by the moon, the same approach may be used if stars are eclipsed by the Earth. Unfortunately, accurate measurement of the time of occultation of a star by the Earth is complicated by the presence of the Earth's atmosphere. The degree to which the Earth's atmosphere degrades the accuracy of these measurements is currently unknown.

IV. Other Sources Considered for Inertial Navigation Updates

In addition to the measurements and sensors described previously, a number of other measurement types have been considered. Unlike the optical methods presented earlier, use of the measurements and sensors listed in the following sections may introduce noteworthy performance limitations in the cislunar regime, require considerable technological maturation before they are implemented in a mission, or necessitate the deployment of significant additional infrastructure. It is likely that a spacecraft may use these navigation techniques during the LEO, LLO, and/or EDL phases of the mission with great success; what is in question here is the suitability (and relative competitiveness compared to the methods listed earlier) of these techniques in cislunar space. Finally, it is worth noting that, with additional work, some of these methods may soon advance to the point where their use in the cislunar regime is more attractive.

A. Planets

To date, little use has been made of planets for navigation purposes in the cislunar regime. Because of the large distances involved as well as the geometric distribution of planets in the plane of the ecliptic, accuracies of a planet-based navigation system will generally be very large relative to other competing solutions. The closest Earth ever comes to another planet is on the order of 0.28 AU (Venus). At these distances, an angular error of only 1 arcsecond results in a position error on the order of 200 km. Additionally, because the spacecraft is already known to be in an Earth (or lunar) orbit, the geometry change over time is not expected to provide any useful information, regardless of the duration. Therefore, observations of a planet provides about the same information as the observation of a star. The primary difference is that planets are not stationary on the celestial sphere (requiring accurate onboard planetary ephemeris data) and planets have a substantially larger apparent diameter.

Even if planets were to be used, only Venus, Mars, Jupiter, and Saturn are practical candidates for navigation purposes (Mercury is too close to the sun and the outer planets are not bright enough). Further, after the planet has been optically detected, the apparent diameter is sufficiently large that a centroiding algorithm is required. The apparent disk of Jupiter as seen from Earth, for example, has a diameter that varies from about 30 to 60 arcseconds.[§] Centroiding may be further complicated by the fact that some of the planets (Venus, in particular) go through phases as observed from the Earth.

Although clearly not appropriate for cislunar navigation, the use of planets has been proposed for interplanetary navigation [40]. The difference is that, for interplanetary trajectories, there are useful changes in geometry as the spacecraft moves throughout the solar system. Such changes are not seen if the spacecraft stays in the Earth–moon system.

B. Optical Satellite Observations

Expanding on the ideas behind the use of natural targets for navigation, optical observations of man-made satellites may be used [41,42]. Instead of taking angles-only optical measurements of the primary body and natural satellites (moons), measurements are taken of artificial satellites for which precise position data are available. Although the process is complex, it may also be possible to obtain an

[§]"Apparent Disk of Solar System Object," Astronomical Applications Dept., U.S. Naval Observatory, http://aa.usno.navy.mil/data/docs/diskmap.php [cited 8 August 2008].

estimate of the range to the target through measurements of the satellite's brightness. Strong candidates for passive targets include GPS satellites [42] and numerous geostationary satellites in well-known orbits. A major challenge with such an approach is the distance at which the target satellite may be optically acquired. Take, for example, results from the space-based visible (SBV) program [43] in which numerous optical measurements were made of various satellites. The SBV sensor was flown on the Midcourse Space Experiment satellite in an 898 km altitude, near sun-synchronous orbit. Measurements of the Telstar 401 and Symphonie A/B satellites in geostationary orbit indicate that magnitudes on the order of 10–15 should be expected at a range on the order of 40,000 km [43]. The authors estimate that a magnitude of 15 corresponds to a 0.5 m^2 cross section at a range of about 40,000 km. Apparent magnitudes are related by

$$m_1 - m_2 = -2.5\log_{10}\left(\frac{f_1}{f_2}\right) \tag{16}$$

where m is the apparent magnitude and f is the flux [44]. Given this relation, along with the fact that the flux will decrease as the inverse square of the distance, if the apparent magnitude of a satellite is known at some distance, the apparent magnitude for the same satellite at some other distance may be calculated. This computation was performed for observations of a geostationary satellite during the lunar return. To bound the region of expected observations, the apparent magnitude of a geostationary satellite as seen by an observer moving along the reference trajectory shown in Fig. 1 was computed for the two bounding extremes indicated earlier ($m = 10$ to $m = 15$ at a range of 40,000 km). The results of this analysis are shown in Fig. 12. These results indicate that it will be very difficult to make optical observations of geostationary satellites during the first 1–2 days of the return trajectory. Based on these results, sensors capable of detecting objects with magnitudes on the order of 18–20 are expected to be necessary for such a solution to be feasible. Here, it is worth noting that, on average, there are more than 4300 stars/deg^2 that are brighter than $m = 18$ and more than 14,700 stars/deg^2 that are brighter than $m = 20$ [45]. With object densities this high, it may be difficult to detect and distinguish a satellite from the background starfield.

Because the brightness of the target spacecraft is a function of the sun–target–spacecraft angle, the performance of such a system will likely be dependent on the date of the lunar return (or, more specifically, the sun–Earth–moon configuration). Further, once a satellite is acquired, it may be difficult to ensure that the correct satellite is being used, especially at large distances when the target spacecraft is faint and difficult to see. Optical beacons or marking may aid in the detection and identification of artificial satellites [46].

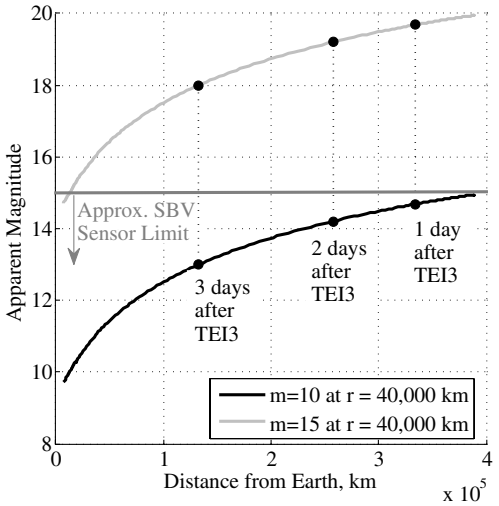

Fig. 12 Apparent magnitude of a geostationary satellite along the nominal lunar return trajectory with time after TEI3 shown for reference.

One of the most significant challenges with using only optical satellite observations is poor geometry. During most of the lunar return, the observable satellites are all in the direction of Earth. As is clear from Fig. 1, this means that the line of sight from the spacecraft to the majority of possible target satellites will be roughly parallel to the return trajectory. This results in poor state knowledge in the radial direction. The emplacement of additional satellites that would create a line of sight perpendicular to the other measurements could significantly improve the navigation solution (satellites placed near the triangular libration points of Earth–moon system may fulfill this need). It will likely be very difficult, however, to obtain measurements out of the Earth–moon plane for the majority of the lunar return trajectory.

It is also necessary to consider the accuracy of optical measurements of satellites. The SBV sensor discussed earlier also took numerous measurements of GPS and GLONASS satellites. Because the positions of these satellites are known with a high degree of accuracy, errors in the SBV measurements may be computed. Results indicated that arcsecond accuracy is achievable with current technology [43].

Finally, the effectiveness of obtaining an instantaneous position fix using only optical observations of Earth-orbiting satellites is investigated. Performance is computed using three to five passive target satellites with altitudes varying from 200 to 20,200 km. The location of the spacecraft along the return trajectory shown in Fig. 1b is randomly selected and then the target satellites are placed in a random geometry subject to the following constraints: 1) the Earth does not disrupt line-of-sight visibility and 2) the target satellite is not between the Earth and the spacecraft (such conditions would make it difficult to optically detect the satellite). This geometry is then used to compute the instantaneous 1σ error ellipse for the spacecraft that could be computed with no a priori information. The results for such an analysis with a measurement accuracy of 1 arcsecond are shown in Fig. 13.

From reviewing the results shown in Fig. 13, it is apparent that poor geometry can create dramatic variations in the achievable accuracy, especially as fewer satellites are visible and as the distance from the Earth increases. There is, however, a clear floor to these variations that puts a limit on the minimum achievable accuracy, regardless of how favorable the geometry may be. Further, as was mentioned briefly earlier, the geometry of the problem is such that the line-of-sight vectors from the spacecraft to the majority of the possible target satellites will all point toward Earth, creating poor resolution in the radial direction.

Finally, although not actually satellites, optical observations such as reflectors or other markers placed on the moon may also be used for navigation. These types of measurements would be similar to the angular surface feature measurements discussed in Sec. III.B.

C. Global Navigation Satellite Systems

The use of global navigation satellite systems has been a popular navigation solution in recent years. Well-known examples of such systems include GPS and GLONASS. These systems consist of a constellation of satellites for which extremely accurate position and timing data are available. Each of the satellites in this constellation continuously transmits data (including precise time and ephemeris information) that may be used for navigation purposes. These signals are observed by a receiver that compares the signal transmit time with the signal arrival time and the resulting time difference is used to calculate the pseudorange. Determining the pseudorange from at least four satellites yields sufficient information to generate an instantaneous three-dimensional position fix and resolve clock bias. It is important to note that, even if enough GPS satellites are not in view to generate an independent position fix, the measurements from one or two satellites may still be fed into a filter that combines these measurements with data from other sensors.

The classic model for pseudorange PR is given by the following expression:

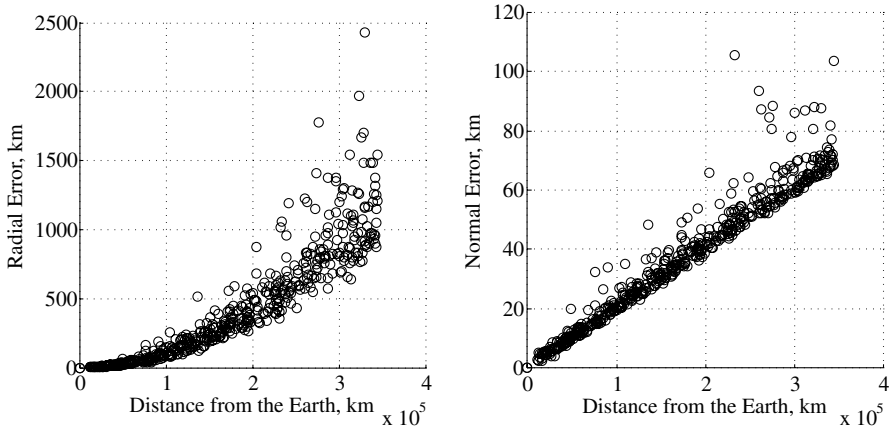

a) Radial error b) Normal error

Fig. 13 Instantaneous position error 1σ from angular measurements of four Earth-orbiting satellites with 1σ accuracy of 1 arcsecond.

$$PR = R + c(\delta t_u - \delta t_s) + I + T + \epsilon_{PR} \tag{17}$$

where R is the geometric range, c is the speed of light, δt_s is the GPS satellite clock error, δt_u is the user clock error, I is the signal delay due to the ionosphere, T is the signal delay due to the troposphere, and ϵ_{PR} is the sum of the remaining errors. In the application of GPS measurements for cislunar navigation, signal delay due to ionosphere and troposphere effects will only be a factor for GPS satellites whose signal grazes the Earth's surface and passes through the atmosphere. In most cislunar navigation applications, however, the signal will not pass through the atmosphere, resulting in no atmosphere related delay: $I = T = 0$. More detailed measurement models may be found in many popular references, such as Misra and Enge [47].

Simply by differentiating Eq. (17), a measurement model for the pseudorange rate may be derived for a direct measurement of velocity:

$$\dot{PR} = \dot{R} + c(\dot{\delta t_u} - \dot{\delta t_s}) + \dot{I} + \dot{T} + \epsilon_{\dot{P}R} \tag{18}$$

$$\dot{PR} = (\mathbf{v}_s - \mathbf{v}_u) \cdot \left(\frac{\mathbf{r}_s - \mathbf{r}_u}{\|\mathbf{r}_s - \mathbf{r}_u\|} \right) + c(\dot{\delta t_u} - \dot{\delta t_s}) + \dot{I} + \dot{T} + \epsilon_{\dot{P}R} \tag{19}$$

where $\mathbf{r}_s$ and $\mathbf{v}_s$ are the position and velocity vectors of the GPS satellite, and $\mathbf{r}_u$ and $\mathbf{v}_u$ are the position and velocity vectors of the user receiver. The pseudorange rate measurement is obtained from measuring the Doppler shift of the received carrier signal. Recall that the range rate measured due to a Doppler shift is given by

$$\dot{R} = \lambda(f_t - f_r) \tag{20}$$

where λ is the wavelength of the transmitted signal, f_t is the frequency of the transmitted signal, and f_r is the frequency of the received signal.

Because the GPS satellite constellation was designed for navigation on Earth, the antennas on these satellites all point toward Earth. This configuration makes it unlikely that a signal of sufficient strength will be available for navigation purposes in cislunar space without the use of a directional antenna to receive the GPS signals. This is especially true if the signal is to be received through one of the side lobes (or back lobe) of the antenna pattern that have a significantly lower signal power. Furthermore, even if a signal could be obtained, the geometry is poor, especially when the spacecraft is near the moon.

If only existing GPS satellites are used for lunar navigation, the geometric dilution of precision (GDOP) along the reference trajectory described in Fig. 1 is as shown in Fig. 14a. Each of the GDOP data points in this figure represent the result of a Monte Carlo analysis where many different GPS satellite configurations were considered. A check was performed to ensure that each GPS satellite used had a clear line of sight to the spacecraft on the lunar return. Further, it was assumed that the spacecraft had a high gain antenna capable of detecting the signal from the side lobes of the GPS antennas. If only the signal from the main lobes were to be used, the geometry would be further restricted and the GDOP would be expected to increase beyond what is reported in Fig. 14a. Note that GDOP increases by multiple orders of magnitude between LEO altitudes and the moon. Therefore, as the sole sensor, it is unlikely that a GPS-based system would be adequate for cislunar navigation without modification. GPS measurements, however, may provide valuable additional data in the proper data fusion environment. More detailed discussions of the accuracy of a GPS-based navigation solution for a spacecraft that approaches or exceeds the altitude of the GPS constellation may be found in the literature [48,49].

It is possible that a new system could be built that is better suited for cislunar navigation. Such a system would likely have assets in both Earth orbit and lunar orbit. Alternatively, the existing GPS infrastructure could be expanded to include satellites in LLO or at one of the Earth–moon libration points (likely L1 or L2). A noticeable improvement in GDOP is observed when only one lunar-orbiting satellite is added. Figure 14b shows the GDOP along the reference lunar return trajectory using the existing earth-orbiting GPS satellites and one GPS-like satellite in lunar orbit. Note the drastic improvement over the system with no lunar-based assets.

The largest obstacle to the implementation of such a system is reception of the signal from the GPS satellites. Further study is required to determine if the signal-to-noise ratio is high enough to reliably acquire a signal from a GPS antenna main lobe and/or side lobe in cislunar space. Additionally, implementation of this system would likely require the deployment of new infrastructure in lunar orbit or at the Earth–moon libration points. There are numerous cost and schedule concerns associated with deploying such a system.

D. Pulsars

Pulsars are new and relatively untested natural targets for spacecraft navigation. Although pulsar-based navigation looks to have a promising future, much work remains to be done in hardware maturation and testing. This low technology readiness makes it unlikely that pulsars will be used as the primary source of navigation for near-term missions. Although much testing remains, a substantial amount of work has been performed in this area [50–53]. Further, pulsars may be an effective way to obtain navigation information outside of the Earth–moon plane. What follows is a brief discussion of the present state of pulsar-based navigation.

Pulsars are highly magnetized and rapidly rotating neutron stars that generate a beam of electromagnetic radiation. This beam of radiation rotates with the star and, to an external observer, creates a pulsed signal as the beam passes over the observer. The pulsating x-ray signatures that result from this phenomenon are typically stable, predictable, and unique. The observed rotational stability,

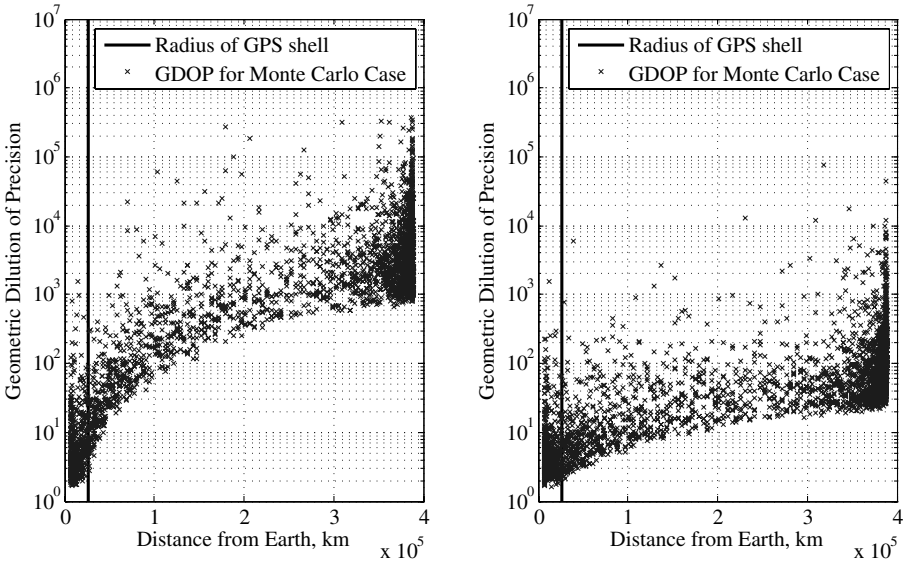

a) GDOP using four existing GPS satellites

b) GDOP using three existing GPS satellites and one new GPS satellite in lunar orbit

Fig. 14 Geometric dilution of precision along reference lunar trajectory.

measurable with fractional uncertainty on the order of 10^{-12}–10^{-15} for some pulsars, is attributed to their high rotational inertia [54]. Some millisecond pulsars are especially stable and are believed to have long-term pulse stability as good as (and possibly better than) that of atomic clocks [55,56]. Comparisons between observed data and pulse timing models for 2 ms pulsars (PSR B1937+21 and PSR B1855+09) have been shown to generate postfit timing residuals with root-mean-square amplitudes below 10^{-6} s [57]. For reference, the pulse profile of PSR B1937+21 is provided in Fig. 15. Note that PSR B1937+21 is the fastest known millisecond pulsar, with a period of 1.557806498(2) ms [58]. Inspection of the pulse profile shows a narrow primary pulse with a duration of approximately 100 μs.

Although determining the range to a pulsar is infeasible, angular information may be precisely determined and the pulsar may be identified by its unique signature. Using only this information, pulsars may be treated as regular stars for navigation purposes. Instead of identifying the star through purely optical means, the unique pulse signature may be used as an identification aid. Then, as discussed in Sec. III.B, angular measurements between the pulsar and a surface feature on the Earth/moon may be used for navigation. The time of occultation of the pulsar (and hence the pulse) may also be used. Unfortunately, because there are only a limited number of usable pulsars, the frequency of pulsar occultations will probably not be sufficient for reliable navigation purposes.

Additional information may be obtained by comparing the time of arrival and the direction of pulses from one or more known pulsars with predicted values from a pulsar timing model. With directional and timing information, other navigation methods are available.

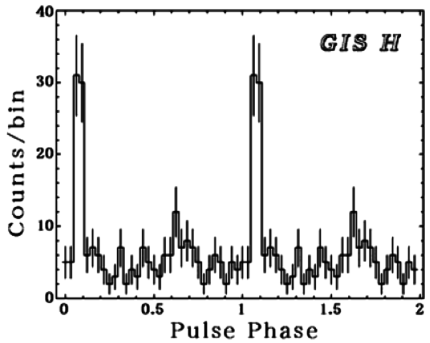

Fig. 15 Pulse profile for PSR B1937+21 (213 photons collected at energy range of 1.7–6.5 keV) [58].

The stable pulsating x-ray time signatures of some pulsars are a unique property that may be used for navigation. If accurate models exist for the observed pulsars, the time of arrival of pulses from multiple pulsars may be used to estimate the spacecraft's absolute position. A notional diagram of this approach is shown in Fig. 16, where the pulsars are assumed to be far enough away from the spacecraft that parallax is neglected. The geometry in Fig. 16 suggests the following measurement model:

$$t = t_{\mathrm{SSB}} - \frac{1}{c}(\mathbf{n}_{\mathrm{star}} \cdot \mathbf{r}) \tag{21}$$

where t is the time of arrival of the pulse at the spacecraft, t_{SSB} is the predicted time of arrival of the pulse at the solar system barycenter (SSB), $\mathbf{r}$ is the position vector of the spacecraft relative to the SSB, c is the speed of light, and $\mathbf{n}_{\mathrm{star}}$ is the unit vector in the direction of the line of sight of the pulsar. The SSB is used because this is a conventional inertial frame chosen for pulsar observations. Including error sources into Eq. (21) yields the following measurement model

$$t = t_{\mathrm{SSB}} - \frac{1}{c}(\hat{\mathbf{n}}_{\mathrm{star}} \cdot \mathbf{r} + \epsilon_{\mathrm{rel}} + \epsilon_{\mathrm{PM}} + \epsilon_{\mathrm{locSSB}}) + b + \tau - \tau_{\mathrm{SSB}} \tag{22}$$

where $\hat{\mathbf{n}}_{\mathrm{star}}$ is as described in Eq. (8), ϵ_{rel} is the position error in the direction of the pulsar due to relativistic effects, ϵ_{PM} is the position error in the direction of the pulsar due to proper motion of the pulsar/SSB, $\epsilon_{\mathrm{locSSB}}$ is the position error in the direction of the pulsar due to error in the location of the SSB, b is the spacecraft clock bias, τ is the error in the measured time of arrival of the pulse at the spacecraft, and τ_{SSB} is the error in the predicted time of arrival of the pulse at the SSB. Sheikh and Pines provide thorough discussion of the error sources given in Eq. (22) [51].

Note that, to determine the absolute position, the specific pulse being measured must be identified. Because the spacecraft is detecting a repeating natural phenomena, there will be an ambiguity regarding which pulse is actually being observed. Sheikh et al. [50] suggest that the spacecraft absolute position may be estimated if the pulse time of arrival and the direction of the pulsar is simultaneously measured for multiple pulsars. The idea behind this is similar in concept to the integer cycle ambiguity-resolution methods used by GPS [47,59].

Further, if an estimate of the spacecraft position is available, the pulse time of arrival may be predicted. Then, using the difference between the observed pulse time of arrival and the predicted time of arrival, a correction to the spacecraft's position (in the direction of the pulsar) may be determined. Sheikh et al. [50] provide a thorough

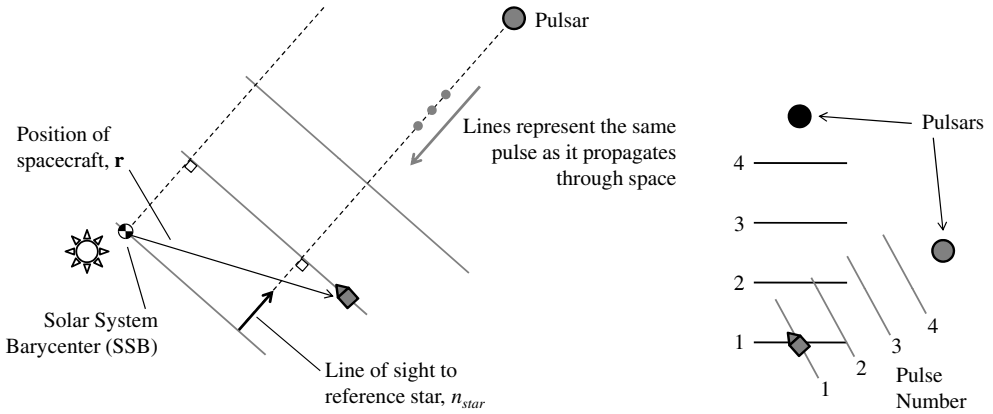

a) Geometry for pulse time of arrival measurements

b) Simultaneous tracking of pulses from multiple pulsars

Fig. 16 Geometry for pulsar-based navigation.

discussion of the measurement model for this approach. The authors use this measurement model to demonstrate pulsar-based navigation using flight measurements from the ARGOS satellite. Their analysis indicates that corrections to spacecraft position with accuracies on the order of 2 km are achievable using the instrumentation available on that mission (detectors sensitive to photons with an energy of 10^{-15} keV and having a time resolution of 2 μs) [50,60].

E. Ranging to Earth or Moon

Because of the proximity of the Earth and the moon, it may be possible to gain useful range information by bouncing a signal off of the surface of one (or both) of these bodies. Recent altimetry missions, such as ICESat [61], have demonstrated that precise ranging measurements are possible, although these methods have only been demonstrated for satellites in LEO. Studies that have investigated the feasibility of ranging by bouncing a signal off the moon have found this to be a demanding task. One such study [9] found that, when the spacecraft is only 16,400 km from the moon, an antenna with a 4 ft diameter is required for microwave ranging. Further, such a method requires detailed knowledge of the planet's surface, time of travel of the signal, and the motion of the spacecraft during the time of travel.

F. Radiometric Tracking

Radiometric tracking is the traditional way that data are collected for inertial state updates in cislunar space. Common systems used for this purpose are the Deep Space Network (DSN) and the Tracking and Data Relay Satellite System (TDRSS). The DSN, for example, operates through radiometric tracking of the spacecraft via a ground-based system [62,63]. Inertial updates are then sent to the vehicle through a communications link. Although this approach does not represent an autonomous source for external navigation updates, it is included for completeness.

It is conjectured that signals from DSN or TDRSS may be used in a passive mode. As an example, consider the Terra spacecraft. This LEO mission used forward-Doppler measurements from the TDRSS satellites to autonomously navigate in real time [64]. Note that, if autonomous navigation is required as a backup for a communication system failure, as is the case for the Orion spacecraft, radiometric tracking may not be a viable option.

Passively transmitting beacons may be placed on satellites or on the Earth/moon surface to act as navigation aids. The signals from such beacons may be used directly for navigation or to help identify a spacecraft. Unlike the satellite navigation systems described separately, these beacons do not transmit data, they are simply used to estimate the range rate with respect to the source. These range-rate measurements would behave in the same manner as described in Eqs. (18–20) for GPS Doppler measurements. It may also be possible to identify the direction to the source using an approach akin to vhf omnidirectional ranging systems commonly used in commercial aviation [65].

V. Conclusions

The most promising measurement sources for autonomous inertial updates in cislunar space are based on observations of natural targets. In general, the lack of abundant man-made assets outside of LEO renders most options relying on observations of human-emplaced infrastructure unrealistic for cislunar navigation early in the lunar program. The best method appears to be angular measurements between reference stars and moon/Earth horizon or surface features.

Briefly consider the implications of these findings on the Orion vehicle that was used as a motivating example in the introduction. The Orion currently has the instrumentation to perform all of the measurements discussed in Sec. III. These sensors, however, were selected primarily for LEO applications. Modifications may be needed to some of the devices to operate them in the necessary dynamic range. It is also expected that sensor fusion and navigation algorithms in the cislunar regime will be different from what is used in LEO or LLO.

Future work will focus on investigating the most promising sources for inertial navigation updates in more detail. Focus will be placed on developing measurement models, identifying sensors, estimating sensor performance, and sensor fusion. This analysis should provide the basis for a "bottom-up" assessment of cislunar navigation performance. Such a bottom-up approach could be used to assess the performance of the instrumentation suite on the Orion or other lunar spacecraft. New sensors could also be added to gain an understanding of how a different sensor suite would affect the quality of the estimated state.

Acknowledgments

The authors thank Christopher D'Souza and Michael Weeks of the NASA Johnson Space Center, Joel Getchius and Emil Schiesser of the Engineering Services Contracting Group, and Sebastian Muñoz and Henri Kjellberg of the University of Texas at Austin. This research was made possible by NASA grant NNX07AP92G.

References

[1] D'Souza, C., Crain, T., Clark, F., and Getchius, J., "Orion Cislunar Guidance and Navigation," AIAA Paper 2007-6681, Aug. 2007.

[2] Hall, R., "Lunar Impact: A History of Project Ranger," NASA SP-4210, 1977.

[3] Lozier, D., Galal, K., Folta, D., and Beckman, M., "Lunar Prospector Mission Design and Trajectory Support," American Astronautical Society Paper 98-323, 1998.

[4] Wollenhaupt, W., "Apollo Orbit Determination and Navigation," AIAA Paper 1970-27, 1970.

[5] Mamich, H., and D'Souza, C., "Orion Preliminary Navigation System Design," AIAA Paper 2008-7295, Aug. 2008.
[6] Proud, R., Hardy, J., Pape, M., and Rosburg, M., "Onboard Automated GN&C Decision-Making Concepts for NASA's CEV," American Astronautical Society Paper 07-074, 2007.
[7] Bate, R., Mueller, D., and White, J., *Fundamentals of Astrodynamics*, Dover, New York, 1971.
[8] Gaylor, D., "Integrated GPS/INS Navigation System Design for Autonomous Spacecraft Rendezvous," Ph.D. Thesis, University of Texas at Austin, Austin, TX, 2003.
[9] Bowers, E., "Requirements for Onboard Optical Guidance of Spacecraft on Lunar Trajectories," *Journal of Spacecraft and Rockets*, Vol. 3, No. 3, 1966, pp. 328–334. doi:10.2514/3.28447
[10] Tuckness, D., and Young, S., "Autonomous Navigation for Lunar Transfers," *Journal of Spacecraft and Rockets*, Vol. 32, No. 2, 1995, pp. 279–285. doi:10.2514/3.26607
[11] Bielkowicz, P., Horrigan, R., and Walsh, R., "Manual Onboard Methods for Orbit Determination," *Journal of Spacecraft and Rockets*, Vol. 8, No. 3, 1971, pp. 284–289. doi:10.2514/3.30261
[12] Action, C., "Processing Onboard Optical Data for Planetary Approach Navigation," *Journal of Spacecraft and Rockets*, Vol. 9, No. 10, 1972, pp. 746–750. doi:10.2514/3.61796
[13] Cesarone, R., "Voyager 1 Saturn Targeting Strategy," *Journal of Spacecraft and Rockets*, Vol. 19, No. 1, 1982, pp. 72–79. doi:10.2514/3.62207
[14] Mastrodemos, N., Kubitschek, D., and Synnott, S., "Autonomous Navigation for the Deep Impact Mission Encounter with Comet Tempel 1," *Space Science Reviews*, Vol. 117, Nos. 1–2, 2005, pp. 95–121. doi:10.1007/s11214-005-3394-4
[15] Stastny, N., and Geller, D., "Autonomous Optical Navigation at Juputer: A Linear Covariance Analysis," AIAA Paper 2006-6680, 2006.
[16] Sabol, C., Carter, S., and Vallado, D., "A Fresh Look at Angles-Only Orbit Determination," American Astronautical Society Paper 99-363, 1999.
[17] Wilcox, J., "Self-Contained Orbital Navigation Systems with Correlated Measurement Errors," *Journal of Spacecraft and Rockets*, Vol. 3, No. 11, 1966, pp. 1585–1591. doi:10.2514/3.28711
[18] Hoag, D., "The History of Apollo On-Board Guidance, Navigation, and Control," *The Eagle has Returned*, edited by E. Steinhoff, Vol. 43, Univelt, San Diego, CA, 1976, pp. 270–300.
[19] Sidi, M., *Spacecraft Dynamics & Control, A Practical Engineering Approach*, Cambridge Univ. Press, Cambridge, England, U.K., 2001.
[20] Tapley, B., Schutz, B., and Born, G., *Statistical Orbit Determination*, Elsevier, New York, 2004.
[21] Brown, R., and Hwang, P., *Introduction to Random Signals and Applied Kalman Filtering*, 3rd ed., Wiley, New York, 1997.
[22] Gelb, A., *Applied Optimal Estimation*, MIT Press, Cambridge, MA, 1974.
[23] Anon., "Apollo Training: Guidance and Control Systems, Block II S/C 101," *Apollo Logistics Training*, NASA, 15 Sept. 1967.
[24] Mathematical Physics Branch, "Apollo 15 Navigation Results," Manned Spaceflight Center Internal Note No. 71-FM-372, Oct. 1971.
[25] "Guidance System Operations Plan for Manned CM Earth Orbital and Lunar Missions Using Program Colossus I (Rev. 237) and Program Colossus IA (Rev. 249), Section 5 Guidance Equations (Rev. 4)," Guidance System Operations Plan No. R-577, Dec. 1968.
[26] Battin, R., "Some Funny Things Happened on the Way to the Moon," *Journal of Guidance, Control, and Dynamics*, Vol. 25, No. 1, 2002, pp. 1–7. doi:10.2514/2.4850
[27] Getchius, J., Crain, T., and D'Souza, C., "Optical Navigation for the Orion Vehicle," American Astronautical Society Paper 08-105, 2008.
[28] Williams, K., Taylor, A., Stanbridge, D., Wol, P., Page, B., Williams, B., and McAdams, J., "Navigation for the MESSENGER Missions First Mercury Encounter," AIAA Paper 2008-6761, 2008.
[29] Liebe, C., "Accuracy Performance of Star Trackers: A Tutorial," *IEEE Transactions on Aerospace and Electronic Systems*, Vol. 38, No. 2, April 2002, pp. 587–599. doi:10.1109/TAES.2002.1008988
[30] Johnson, A., Ansar, A., Matthies, L., Trawny, N., Mourikis, A., and Roumeliotis, S., "A General Approach to Terrain Relative Navigation for Planetary Landing," AIAA Paper 2007-2854, 2007.
[31] Adams, D., Criss, T., and Shankar, U., "Passive Optical Terrain Relative Navigation Using APLNav," Inst. of Electrical and Electronics Engineers Paper No. 1646, May 2008.
[32] Osenar, M., Clark, F., and D'Souza, C., "Performance of an Automated Feature Tracking Lunar Navigation System," American Astronautical Society Paper 08-101, 2008.
[33] Jones, B., "Surface Feature Navigation in Low Lunar Orbit," American Astronautical Society Paper 08-104, 2008.
[34] Hanak, C., "Lost in Low Lunar Orbit Crater Pattern Detection and Identification," Ph.D. Dissertation, Univ. of Texas at Austin, Austin, TX, May 2009.
[35] Levine, G., "A Method of Orbital Navigation Using Optical Sightings to Unknown Landmarks," *AIAA Journal*, Vol. 4, No. 11, 1966, pp. 1928–1931. doi:10.2514/3.3820
[36] Toda, N., and Schlee, F., "Autonomous Orbital Navigation by Optical Tracking of Unknown Landmarks," *Journal of Spacecraft and Rockets*, Vol. 4, No. 12, 1967, pp. 1644–1648. doi:10.2514/3.29147
[37] Keenan, R., and Regenhardt, J., "Star Occultation Measurements as an Aid to Navigation in Cis-Lunar Space," M.S. Dissertation, Massachusetts Inst. of Technology, Cambridge, MA, June 1962.
[38] Landgraf, M., Thiele, G., Koschny, D., and Udrea, B., "Optical Navigation for Lunar Exploration Missions," International Astronautical Congress Paper IAC-06-C.1.7.5, Oct. 2006.
[39] Psiaki, M., and Hinks, J., "Autonomous Lunar Orbit Determination Using Star Occultation Measurements," AIAA Paper 2007-6657, 2007.
[40] Vasile, M., Romano, M., and Trainiti, F., "An Optical Based Strategy for Deep Space Autonomous Navigation," ESA Paper No. SP-425Oct. 1999.
[41] Lambour, R., Bergemann, R., von Braun, C., and Gaposchkin, E., "Space-Based Visible Space Object Photometry: Initial Results," *Journal of Guidance, Control, and Dynamics*, Vol. 23, No. 1, 2000, pp. 159–164. doi:10.2514/2.4504
[42] Fliegel, H., and Warner, L., "Photometry of Global Positioning System Block II and IIA Satellites on Orbit," *Journal of Spacecraft and Rockets*, Vol. 38, No. 4, 2001, pp. 609–616. doi:10.2514/2.3725
[43] Stokes, G., von Braun, C., Sridharan, R., Harrison, D., and Sharma, J., "Space-Based Visible Program," *Lincoln Laboratory Journal*, Vol. 11, No. 2, 1998, pp. 205–238.
[44] Schulman, E., and Cox, C., "Misconceptions About Astronomical Magnitudes," *American Journal of Physics*, Vol. 65, No. 10, 1997, pp. 1003–1007. doi:10.1119/1.18714
[45] Allen, C., *Astrophysical Quantities*, Athlone Press, London, 3rd ed., 1973.
[46] Hayhurst, T., Osibov, M., Russell, R., Maulfair, R., and Fleeter, R., "Simple, Inexpensive Optical Beacon for Use on Small Satellites," *Journal of Spacecraft and Rockets*, Vol. 28, No. 1, 1991, pp. 58–63. doi:10.2514/3.26209
[47] Misra, P., and Enge, P., *Global Positioning System: Signals, Measurements, and Performance*, 2nd ed., Ganga-Jamuna Press, Lincoln, MA, 2006.
[48] Holt, G., and Lightsey, E., "In Situ Navigation of Spacecraft Formations in High-Altitude and Extraterrestrial Orbits," *Journal of Spacecraft and Rockets*, Vol. 45, No. 2, 2008, pp. 299–308. doi:10.2514/1.29361
[49] Carpenter, J., Folta, D., Moreau, M., and Quinn, D., "Libration Point Navigation Concepts Supporting the Vision for Space Exploration," AIAA Paper 2004-4747, 2004.
[50] Sheikh, S., Pines, D., Ray, P., Wood, K., Lovellette, M., and Wol, M., "Spacecraft Navigation Using X-Ray Pulsars," *Journal of Guidance, Control, and Dynamics*, Vol. 29, No. 1, 2006, pp. 49–63. doi:10.2514/1.13331
[51] Sheikh, S., and Pines, D., "Recursive Estimation of Spacecraft Position and Velocity Using X-Ray Pulsar Time of Arrival Measurements," *Navigation: Journal of the Institute of Navigation*, Vol. 53, No. 3, 2006, pp. 149–166.
[52] Sala, J., Urruela, A., Villares, X., Estalella, R., and Paredes, J., "Feasibility Study for a Spacecraft Navigation System Relying on Pulsar Timing Information, Final Report," ESA Advanced Concepts Team, ARIADNA Study 03/4202, 2004.
[53] Hanson, J., "Principles of X-Ray Navigation," Ph.D. Thesis, Stanford Univ., Palo Alto, CA, 1996.
[54] Kaspi, V., "High-Precision Timing of Millisecond Pulsars and Precision Astrometry," *International Astronomical Union, Symposium No. 166: Astronomical and Astrophysical Objectives of Sub-Milliarcescond Optical Astrometry*, Kluwer Academic, Dordrecht, The Netherlands, 1995, pp. 163–171.

[55] Taylor, J., "Millisecond Pulsars: Nature's Most Stable Clocks," *Proceedings of the IEEE*, Vol. 79, No. 7, 1991, pp. 1054–1062. doi:10.1109/5.84982

[56] Matsakis, D., Taylor, J., and Eubanks, T., "A Statistic for Describing Pulsar and Clock Stabilities," *Astronomy and Astrophysics*, Vol. 326, 1997, pp. 924–928.

[57] Kaspi, V., Taylor, J., and Ryba, M., "High-Precision Timing of Millisecond Pulsars, III: Long-Term Monitoring of PSRs B1885+09 and B1937+21," *Astrophysical Journal*, Vol. 428, No. 2, 1994, pp. 713–728. doi:10.1086/174280

[58] Takahashi, M., Shibata, S., Gunji, S., Sakurai, H., Torii, K., Saito, Y., Kawai, N., Dotani, T., and Hirayama, M., "Detection of Pulsed X-Ray Emission from the Fastest Millisecond Pulsar PSR B1937+21 with ASCA," *Astronomische Nachrichten*, Vol. 320, Nos. 4–5, 1999, p. 340. doi:10.1002/1521-3994(199908)320:4/5<340::AID-ASNA340>3.0.-CO;2-B

[59] Teunissen, P., De Jonge, P., and Tiberius, C., "Performance of the LAMBDA Method for Fast GPS Ambiguity Resolution," *Navigation: Journal of the Institute of Navigation*, Vol. 44, No. 3, 1997, pp. 373–400.

[60] Ray, P., Wood, K., Fritz, G., Hertz, P., Kowalski, M., Johnson, W., Lovellette, M., Wol, M., Yentis, D., Bandyopadhyay, R., et al., "The USA X-Ray Timing Experiment," *Proceedings of X-Ray Astronomy*, American Inst. of Physics, CP-599, 2001, pp. 336–345.

[61] Zwally, H., Schutz, B., Abdalati, W., Abshire, J., Bentley, C., Brenner, A., Bufton, J., Dezio, J., Hancock, D., Harding, D., Herring, T., Minster, B., Quinn, K., Palm, S., Spinhirne, J., and Thomas, R., "ICESat's Laser Measurements of Polar Ice, Atmosphere, Ocean, and Land," *Journal of Geodynamics*, Vol. 34, 2002, pp. 405–445. doi:10.1016/S0264-3707(02)00042-X

[62] Moyer, T., *Formulation for Observed and Computed Values of Deep Space Network Data Types for Navigation*, Wiley, Hoboken, NJ, 2003.

[63] Thornton, C., and Border, J., *Radiometric Tracking Techniques for Deep Space Navigation*, Wiley-Interscience, New York, 2003.

[64] Gramling, C., Lorah, J., Santoro, E., Work, K., and Chambers, R., "Preliminary Operational Results of the TDRSS Onboard Navigation System (TONS) for the Terra Mission," *15th International Symposium on Spaceflight Dynamics*, NASA Goddard Space Flight Center, Greenbelt, MD, June 2000.

[65] Kayton, M., and Fried, W., Avionics Navigation Systems, 2nd ed., Wiley, New York, 1997.

D. Spencer
Associate Editor